Application of the speleothem calcium isotope paleo-rainfall proxy to the 8.2 kyr event in coastal California

By

Cameron de Wet

Thesis

Submitted to the Faculty of the

Graduate School of Vanderbilt University

in partial fulfillment of the requirements

for the degree of

MASTER OF SCIENCE

in

Earth and Environmental Sciences

August 31, 2019

Nashville, Tennessee

Approved:

Jessica L. Oster, Ph.D

John C. Ayers, Ph.D

ACKNOWLEDGEMENTS

I would like to thank Elli Ronay for her encouragement and good cheer and the Vanderbilt EES department for fostering such a positive and supportive educational environment. I would also like to thank Dr. Jessica Oster for her patient mentorship and insightful guidance over these last two years.

This work was funded by the National Science Foundation under grant 1554998.

TABLE OF CONTENTS

Page

ACKNOWLEDGEMENTS i

LIST OF TABLES iii

LIST OF FIGURES iv

Chapter

1. INTRODUCTION 1

    1.1 The 8.2 kyr event 1

    1.2 Prior calcite precipitation and the $\delta^{44/40}Ca$ rainfall proxy 2

    1.3 Study site and sample background 4

2. METHODS 6

    2.1 U-series chronology 6

    2.2 Speleothem and cave system calcium isotope data 6

3. RESULTS 8

4. DISCUSSION 12

    4.1 Interpreting the WMC1 $\delta^{44/40}Ca$ record 12

    4.2 Comparisons between speleothem $\delta^{44/40}Ca$ records of the 8.2 kyr event at WMC and Heshang Cave 17

    4.3 Quantitative modeling prior calcite precipitation and rainfall amount at WMC 18

5. CONCLUSIONS 20

REFERENCES 22

LIST OF TABLES

Table Page

1. WMC dripwater $\delta^{44/40}$Ca data. 9
2. WMC glass plate $\delta^{44/40}$Ca data 9
3. WMC host rock $\delta^{44/40}$Ca data 10
4. WMC speleothem $\delta^{44/40}$Ca data 10

LIST OF FIGURES

Figure Page

1. Schematic of prior calcite precipitation (PCP) above a stalagmite....3
2. Map of WMC study area and regional climatology and speleothem records....4
3. WMC map....5
4. Distribution of $\delta^{44/40}$Ca values for WMC and Heshang Cave dripwaters, host rock, plate calcite, and speleothems....12
5. Timeseries of stalagmite WMC1 $\delta^{44/40}$Ca data....13
6. Timeseries of WMC1 Mg/Ca, P/Ca, δ^{13}C, and $\delta^{44/40}$Ca data over the course of the 8.2 kyr event....15
7. Timeseries of Kaite Cave δ^{18}O and WMC1 δ^{13}C and $\delta^{44/40}$Ca data over the course of the 8.2 kyr event....16
8. Timeseries of WMC1 and Heshang Cave $\delta^{44/40}$Ca data over the 8.2 kyr event....17
9. Schematic showing the aspects of the cave system that are input parameters for the Rayleigh fractionation model....18
10. Modeled *f* values for measured WMC and Heshang Cave host rock and speleothem $\delta^{44/40}$Ca data....20

1. INTRODUCTION

1.1 The 8.2 kyr event

Beginning ~8200 years ago, an oxygen isotope excursion of 1-2‰ noted in the Greenland ice cores suggests an abrupt drop in temperature that lasted ~160 years (Alley et al. 1997; Thomas et al. 2007). Paleoclimate proxy records suggest that this decrease in temperature was felt around the North Atlantic region and accompanied by disruptions to precipitation patterns around the globe (Morrill et al. 2013a). It is hypothesized that these changes were caused by suppressed Atlantic Meridional Overturning Circulation (AMOC), possibly driven by the catastrophic draining of proglacial lakes Agassiz and Ojibway into the North Atlantic during the retreat of the Laurentide Ice Sheet (Wiersma and Renssen 2006). However, modeling efforts have been unable to simulate the magnitude and duration of the event documented in proxy records with lake discharge alone (Morrill et al. 2013b). Recent work indicates that AMOC response to a longer-term acceleration of meltwater input to the North Atlantic after the collapse of the Laurentide ice saddle aligns more accurately with climate response to the 8.2 kyr event from proxy records (Matero et al. 2017).

Proxy evidence indicates drier conditions in the Northern Hemisphere tropics and wetter conditions over Northern Europe and parts of the Southern Hemisphere tropics over the 8.2 kyr event (Morrill et al. 2013a). However, since the ~160 year duration of the event is comparable to the range of chronological uncertainty of most paleoclimate proxies, the task of identifying and detailing the expression of the event in records like lake or marine sediment cores has been challenging. Speleothems have been an essential paleoclimate archive for understanding this event due to their ability to be precisely dated using the U-series geochronology. Specifically, speleothem $\delta^{18}O$ records from China, Brazil, and Oman document a southward shift of the Intertropical Convergence Zone (ITCZ) during the 8.2 kyr event, driving strengthened monsoon conditions in much of the Southern Hemisphere tropics and relative aridity in Central America and central China (Cheng et al. 2009). Despite this important information, the 8.2 kyr event has been poorly characterized in western North America due to a paucity of records with sufficient temporal resolution. Recently, stable isotope and trace element records from a White Moon Cave (WMC) speleothem suggest increased wetness and storminess in coastal California during the 8.2 kyr event (Oster et al. 2017). However, these traditional speleothem proxies lack the ability to demonstrate how large these changes in rainfall actually were. The development of quantitative records of rainfall is an important next step for understanding the magnitude of extreme climate perturbations like the 8.2 kyr event, and of speleothem paleoclimatology in general (Wong and Breeker 2015).

Calcium isotope ratios within speleothem carbonate ($\delta^{44/40}Ca$) are thought to respond to changes in the amount of secondary carbonate precipitation that occurs along the seepage water flow path above a speleothem. This parameter has been tested as a potentially quantitative proxy for past effective precipitation and used to reconstruct precipitation variability during the 8.2 kyr event at Heshang Cave in central China (Owen et al., 2016). Here, I build upon the previous

work at White Moon Cave from Oster et al. (2017) by applying the $\delta^{44/40}Ca$ proxy to the study of the 8.2 kyr event record in a WMC stalagmite (WMC1). I compare the new calcium isotope record to the existing $\delta^{18}O$, $\delta^{13}C$, and trace element records from stalagmite WMC1 to test the hypothesis that WMC experienced a wetter and stormier climate during the 8.2 kyr event and to quantify the magnitude of precipitation change over this interval. In doing so, I explore the utility of this proxy in a different climate regime (semi-arid vs. humid monsoonal) and a different host rock geology (marble vs. limestone) than Heshang Cave and attempt to place some constraints on how to apply to this proxy across a range of cave environments. I find that, while promising, important questions remain as to how this new proxy can be applied in cave systems across climatic and geological gradients.

1.2 Prior calcite precipitation and the $\delta^{44/40}Ca$ rainfall proxy

In the soil zone above a cave, carbon dioxide produced by microbial respiration dissolves into soil water. This acidic water seeps downward into the upper epikarst, dissolving calcium carbonate from the bedrock. As this water percolates through the epikarst above a cave system it may encounter pore spaces or fractures with lower pCO_2 than the zone of carbonate dissolution, leading to the degassing of CO_2 and the precipitation of carbonate in these voids, a process termed prior calcite precipitation (PCP) (Fairchild et al. 2000; Owen et al. 2016). The amount of PCP that occurs can be related, to a first approximation, to the amount of local rainfall and groundwater infiltration. More (less) rainfall might lead to a shorter (longer) groundwater residence time and fewer (more) air-filled pore spaces, which allows for less (more) PCP to occur in the epikarst (Cruz et al. 2007; Tooth and Fairchild 2003; Fairchild and Treble 2009).

The concentration of various trace elements (such as Mg, Sr, and Ba) in speleothems has been shown to vary in response to changes in PCP amounts and, by extension, local effective rainfall amounts, due to the preferential removal of Ca relative to trace elements from the groundwater solution during PCP (e.g. Tremain and Froelich 2013). Recent efforts have explored the potential for trace element records to be interpreted quantitatively using modern climate data for calibration, but this approach is limited by the necessity of very high-resolution speleothem laminations and uninterrupted speleothem growth into the modern period, as well as a sufficiently long calibration period (Warken et al. 2018). The development of robust and broadly applicable quantitative records of past rainfall from speleothems remains an important, if still elusive, goal in the field of speleothem paleoclimatology.

Recently, speleothem calcium isotope composition ($\delta^{44/40}Ca$ or $\delta^{44/42}Ca$) has been explored as a new, potentially quantitative, proxy for PCP and effective rainfall (Owen et al., 2016). The $\delta^{44/40}Ca$ proxy is based on the observation that Ca in dripwaters entering a cave tend to be enriched in the heavier Ca isotopes relative to the host rock $\delta^{44/40}Ca$ value, which the water would initially obtain through carbonate dissolution (Owen et al. 2016). This enrichment is interpreted to be driven by PCP wherein the lighter Ca isotopes preferentially enter the secondary carbonate precipitate (fig. 1) (Gussone et al. 2005; Reynard et al. 2011; Tang et al. 2008). Thus, speleothem $\delta^{44/40}Ca$ should provide a new geochemical proxy to assess the amount of PCP that

has occurred at a given time, which can be related to the amount of local effective rainfall (Owen et al., 2016). Furthermore, the cycling of Ca ions during PCP can be thought of as a Rayleigh fractionation process and the amount of PCP can be quantitatively related to the amount of rainfall using a series of transfer functions developed through the study of the modern climate and cave system. Such a model has been developed for and tested in the monsoonal climate of central China (Owen et al., 2016; Li et al., 2018). Here I also evaluate a similar model in the White Moon Cave system, which differs from the Chinese cave both in climate (Mediterranean versus summer monsoonal) and host rock geology (marble versus limestone).

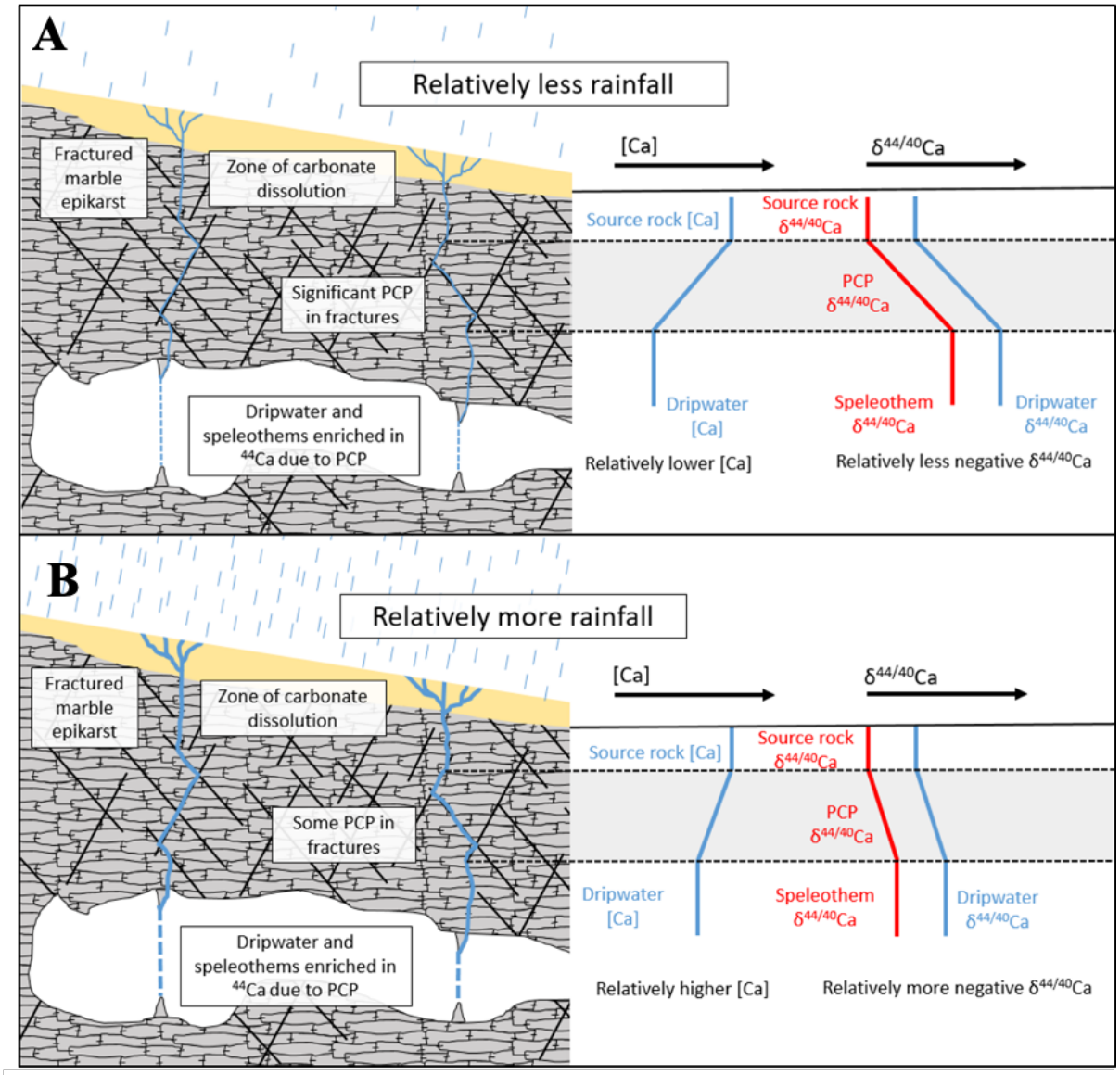

Figure 1. Schematic of prior calcite precipitation (PCP) above a stalagmite and Ca concentration and Ca isotope evolution of dripwater and instantaneous precipitate under different rainfall regimes. **(A)** A period of relatively less rainfall, which results in more PCP and relatively less negative speleothem $\delta^{44/40}$Ca values. **(B)** A period of relatively more rainfall, which results in less PCP and relatively more negative speleothem $\delta^{44/40}$Ca values. Adapted from Owen et al. 2016.

1.3 Study site and sample background

White Moon Cave is situated in a pocket of fracture-dominated, late Paleozoic marble in the Santa Cruz Mountains east of Davenport, CA (N37°00', W122°11'; fig. 2). The modern cave entrance lies within a 20th century quarry that transects the natural cave. The quarry is bordered by Cretaceous quartz diorite (qd) and upper Miocene Santa Margarita sandstone (Tsm) (fig. 2).

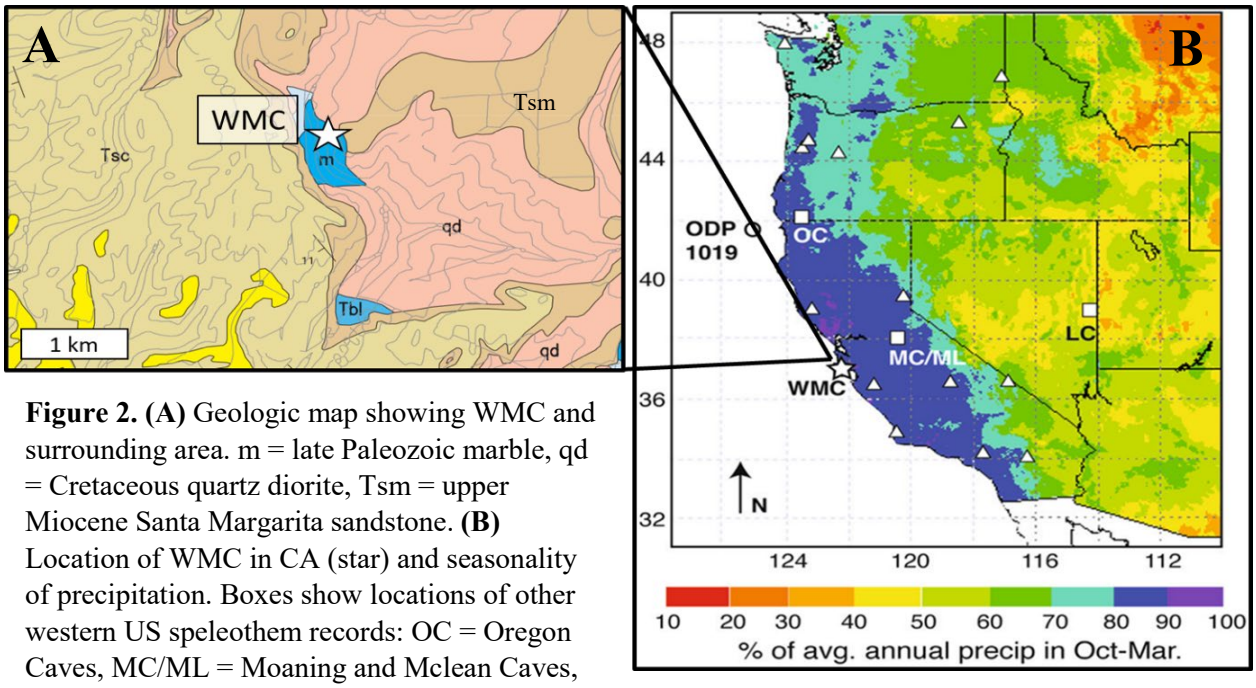

Figure 2. (A) Geologic map showing WMC and surrounding area. m = late Paleozoic marble, qd = Cretaceous quartz diorite, Tsm = upper Miocene Santa Margarita sandstone. **(B)** Location of WMC in CA (star) and seasonality of precipitation. Boxes show locations of other western US speleothem records: OC = Oregon Caves, MC/ML = Moaning and Mclean Caves, LC = Lehman Caves. Circle shows location of ODP drill core 1019. Triangles show locations where event-scale $\delta^{18}O$ of precipitation has been analyzed. Background map shows percent of average annual precipitation (1981-2010) that occurs during the cool season (Oct.-Mar.) based on data from the PRISM Climate Group at Oregon State University. Map is from Oster et al. (2017).

The cave site is characterized by a warm-summer Mediterranean climate and receives an average of 800 mm of precipitation per year, >80% of which falls during the cool season (Oct. to Mar.; fig. 2B). The amplitude of seasonal temperature variability is moderated by the cave's coastal location and thus is relatively small (11.3 - 18°C; Arguez et al. 2010). Cool season rain is sourced primarily from winter storms that tend to originate in the northern or mid-latitude Pacific. However, the region can be influenced by extra-tropical cyclones that source moisture from the central or eastern tropical Pacific. These systems can develop narrow streams of water vapor concentrated near the surface, termed atmospheric rivers, that are associated with significant flooding along the California coast (Dettinger 2011). For comparison, Heshang Cave, China is situated in Cambrian dolomite and receives average annual rainfall of 1144 mm per year, the majority of which falls during the summer monsoon season (May-Oct.) (Hu et al. 2008).

Stalagmite WMC1 is 25.5 cm tall and was collected >820 feet from the modern cave entrance in the quarry wall. The stalagmite grew from ~8600 until at least ~239 cal. years BP 1950. Only the portion of the stalagmite that grew from 8600 to 6850 cal. years BP is analyzed in this study because my focus is on the 8.2 kyr event. Petrographic analysis shows that WMC1 consists of calcite with an elongated columnar fabric intercalated with fine layers of silicate detritus. Elongated columnar fabrics of this sort have been linked to high seepage water

discharge and are often associated with speleothems from caves developed within rocks that contain dolomite or other high-Mg phases (Frisia et al. 2000; Frisia 2015).

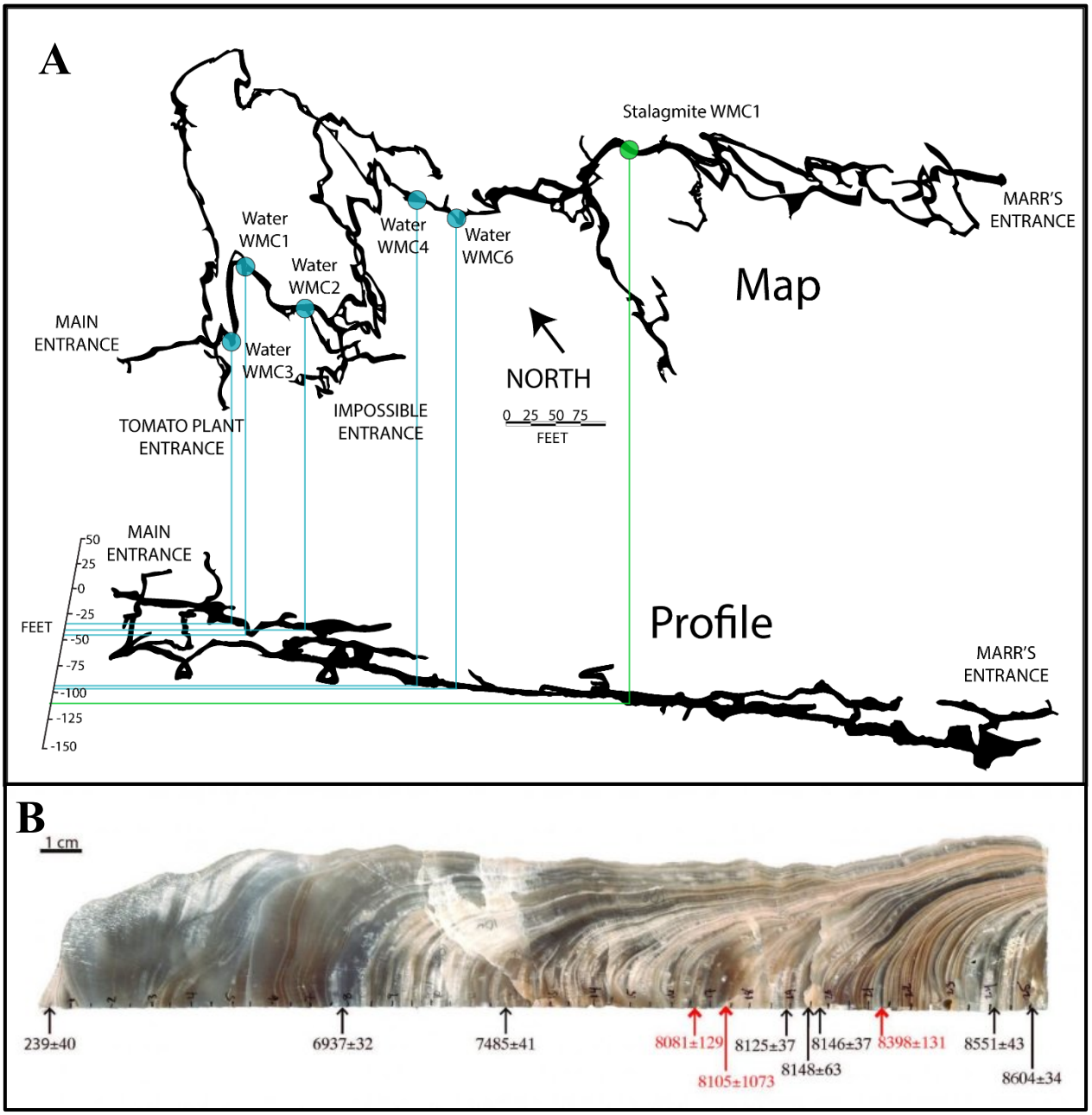

Figure 3. (A) WMC map and profile. Blue dots show drip site locations from this study. Green dot shows approximate location of stalagmite WMC1. Main entrance is the modern entrance, which opens to the quarry wall. Map based on unpublished cartography by P. Bosted in 1986. **(B)** Quartered and polished stalagmite WMC1 with U/Th dates (cal. years BP) and 2 sigma errors from Oster et al. (2017). Dates colored red have high ^{232}Th, have high measured uncertainties, and were not included in the age model.

2. METHODS

2.1 U-series chronology

Eleven sub-samples from stalagmite WMC1 were collected and analyzed for $^{230}Th/U$ dating. The samples were dissolved in 7 N HNO_3 and equilibrated with a mixed spike containing ^{229}Th, ^{233}U, and ^{236}U. U and Th were separated with a two-stage HNO_3-HCl cation exchange procedure, followed by treatment with a mixture of HNO_3 and $HClO_4$ to remove any residual organic matter. U and Th fractions were analyzed using a Thermo Neptune Plus MC-Thermal Ionization Mass Spectrometer at the Berkeley Geochronology Center. Mass fractionations were determined using the gravimetrically determined $^{233}U/^{236}U$ ratio of the spike. Measured peak heights were corrected for peak tailing, instrumental backgrounds, ion counter yields, interfering isotopes spikes, procedural blanks, mass fractionation, and multiplier dark noise/Faraday baselines.

Three samples had high ^{232}Th concentrations and unfavorable $^{232}Th/^{238}U$ ratios ($^{232}Th/^{238}U > 0.001$) and thus were not included in the age model, though they were used to help constrain the appropriate detritus correction. The age-depth model was constructed using the StalAge algorithm from Scholz and Hoffmann (2011). The $^{230}Th/U$ dating of this sample is fully described in Oster et al. (2017).

2.2 Speleothem and cave system calcium isotope data

Sixty-nine ~5 mg samples of speleothem calcite from WMC1 were analyzed for $\delta^{44/40}Ca$ between March 2018 and May 2019. Samples for $\delta^{44/40}Ca$ were drilled from one face of the quartered stalagmite using a handheld dental drill. Twenty-four speleothem samples were collected from the portion of the stalagmite that grew during the 8.2 kyr event (8226 to 8041 cal. yr. BP), yielding sub-decadal temporal resolution over the course of the event. Fourteen speleothem samples were collected from the portion of the speleothem that grew before the 8.2 kyr event (8588 to 8226 cal. yr. BP) and 32 samples were collected from the portion the grew after the event (8041 to 6852 cal. yr. BP), yielding a multi-decadal temporal resolution before and after the event.

Drip waters were collected for $\delta^{44/40}Ca$ analysis from five drip sites within WMC. Water collection sites WMC1 and WMC3 are ~100 feet and ~150 feet from the modern cave entrance in the quarry wall respectively and between 30 and 50 feet deeper than the modern entrance (fig. 3A). Water collection sites WMC1 and WMC3 have been monitored for O and H isotopes as well. This information is described in Oster et al. (2017). These sites were originally chosen for monitoring because they appeared active throughout the year and are easily accessible from the cave entrance. Drip water has also been collected from drip site WMC2, which is ~200 feet from the modern cave entrance and ~40 feet deeper than the modern entrance, though these samples have not been analyzed (fig. 3A). Water collection sites WMC4 and WMC6 are ~545 and ~570 feet from the modern cave entrance respectively and ~95 feet deeper than the entrance (fig. 3A).

The section of the cave where stalagmite WMC1 is from is ~110 feet deeper than the modern entrance, 60-80 feet deeper than drip sites WMC3, WMC1, and WMC2, and ~15 feet deeper than drip sites WMC4 and WMC6 (fig. 3A). I began collecting water samples from drip sites WMC4 and WMC6 for $\delta^{44/40}$Ca analysis because these sites are more similar in vertical depth from the entrance to the section of the cave where stalagmite WMC1 is from. The length of the groundwater flow path above a drip site is a function of the depth of that site and may play a significant role in determining the amount of PCP that can occur above a particular water sampling site. Since water collection sites WMC4 and WMC6 are more similar in depth to stalagmite WMC1, I anticipate that $\delta^{44/40}$Ca data from these two sites will provide more accurate comparisons to the stalagmite WMC1 $\delta^{44/40}$Ca data than data from sites WMC1 and WMC3.

Drip water samples from sites WMC1 and WMC3 collected in March 2017 were analyzed for $\delta^{44/40}$Ca in March 2018. Drip water samples from sites WMC1 and WMC3 collected in June 2018 were analyzed for $\delta^{44/40}$Ca in December 2018. Drip water samples from WMC1, WMC3, WMC4, and WMC6 were collected in February and June 2019 and will be analyzed in July 2019. Drip site WMC2 was not active in February or June 2019.

In order to investigate Ca isotope systematics in the modern cave system, modern calcite was grown on artificial substrates at five locations within the cave. Artificial substrates (frosted glass plates) were installed at WMC1 and WMC2 in February 2014 (fig. 3A). These plates were collected in June 2018. Approximately 1 mg of calcite powder was scraped off of the surface of the glass plates with a scalpel for analysis in November 2018. A new plate were installed at drip site WMC1 in June 2018 and collected in February 2019 and will be analyzed in July 2019. Additional plates were installed at drip sites WMC1 and WMC3, as well as at drip sites WMC4 and WMC6, in February 2019 (fig. 3A). These were collected in June 2019, and will also be analyzed in July 2019.

Three samples of marble host rock were collected from pieces of float in the modern quarry outside of the cave entrance. Powders were drilled from fresh surfaces of the marble hand samples using a handheld dental drill. The three marble samples contain zones with variable amounts of mica and were chosen to represent the variation in the marble host rock observable in float outside of WMC and within the cave itself.

The $\delta^{44/40}$Ca data for all samples were collected at the University of Cambridge using a Thermo Scientific Triton Plus MC-Thermal Ionization Mass Spectrometer. Sample aliquots were combined with a ^{42}Ca-^{48}Ca double-spike at a ratio of 10-1 (sample-to-spike) following the methods of Bradbury and Turchyn (2018). Samples were analyzed for ^{40}Ca, ^{42}Ca, ^{43}Ca, ^{44}Ca, and ^{48}Ca. Data are reported in $\delta^{44/40}$Ca notation relative to the bulk silicate earth (BSE) standard. The data were corrected to account for the long-term average drift of the standards values due to known cup degradation. The calcium isotope data from Owen et al. (2016) presented here for comparison were converted from $\delta^{42/40}$Ca to $\delta^{44/40}$Ca following the guidelines from Heuser et al. (2016) and are presented relative to the BSE standard.

Duplicate analyses were completed for dripwater, glass plate, and host rock samples, with one dripwater duplicate from the March 2018 set being discarded due to instrument instability.

One speleothem sample, AC282, produced a $\delta^{44/40}Ca$ value of 0.082‰ in March 2018, which is an outlier relative to the other speleothem samples analyzed. AC282 was rerun in May 2019 and yielded a new $\delta^{44/40}Ca$ value of -0.4947‰, which is reported instead.

3. RESULTS

WMC1 dripwater $\delta^{44/40}Ca$ values range from -0.29‰ in March 2017 to -0.42‰ in June 2018 with an average value of -0.36‰. WMC3 dripwater $\delta^{44/40}Ca$ values from March 2017 and June 2018 are within analytical uncertainty (-0.28‰ and -0.29‰ respectively; table 1). Glass plate calcite collected in June 2018 from WMC1 has a $\delta^{44/40}Ca$ values of -0.79‰. Glass plate calcite collected in June 2018 from WMC2 has a $\delta^{44/40}Ca$ value of -0.85‰ (table 2). Measured $\delta^{44/40}Ca$ values for WMC marble host rock samples are variable between samples with different amounts of accessory mica phases, ranging from -0.27‰ to -0.59‰ with an average value of -0.5‰ (table 3). The average external 2σ standard deviation over the analysis period on the standard NIST915B was 0.09‰. This value is larger than the 2σ of measured sample replicates for any individual sample and so it is the value that I report as the error for the dataset as a whole.

Using dripwater data from March 2017 and data from the glass plate that was collected in June 2018, and assuming that the single-day dripwater data is representative of period of time that the glass plate was installed, the Ca isotope fractionation at water collection site WMC1 is $\Delta^{44/40}Ca_{calcite\text{-}aq}$ = -0.51‰. This value is less negative than the measure of Ca isotope fractionation at drip site HS4 in Heshang Cave ($\Delta^{44/40}Ca$ = -1.3‰) and at the less negative end of the range of values from laboratory calculations (-1.47‰ < $\Delta^{44/40}Ca$ < -0.46‰; Tang et al. 2008).

A site-specific isotopic fractionation factor (α) between calcite and water can be calculated for a drip site using the drip water and glass plate calcite data:

$$\alpha = (1000+r_d) / (1000+r_s)$$

where r_d is the Ca isotope ratio in the dripwater ($r_d = \delta_{drip}/1000+1$), r_s is the Ca isotope ratio in the precipitate ($r_s = \delta_{CaCO3}/1000+1$). Using dripwater data from March 2017 and data from the glass plate that was collected in June 2018 the fractionation factor (α) at drip site WMC1 is 0.9995. At this stage WMC1 is the only drip site for which I have both drip water and glass plate $\delta^{44/40}Ca$ data and so it is the only site where α can be calculated.

Speleothem $\delta^{44/40}Ca$ values from WMC1 range from -1.20‰ to -0.40‰ with an average value of -0.90‰. The data display decadal-scale variability that is generally within the 2σ of NIST915B. However, there are short-lived excursions within the record, as well as significant oscillations between more negative and more positive values. For example, between ~8328 and ~8376 cal. years BP, speleothem $\delta^{44/40}Ca$ values shift from -0.68‰ to more negative values of -1.20‰ and -1.01‰ and then back to the more positive values of -0.76‰ and -0.73‰ over approximately 50 years. Due to lower sampling resolution before and after the 8.2 kyr event, we

are not able to investigate variability at a sub-decadal scale. However, between 8226 and 8041 cal. years BP we do observe sub-decadal variability, including rapid oscillations between relatively more negative and relatively more positive values during the middle portion of the 8.2 kyr event (8212 to 8141 cal. years BP). Speleothem $\delta^{44/40}$Ca values then increase steadily from -1.036‰ at ~8136 cal. years BP to -0.535‰ by ~8082 cal. years BP before decreasing again to significantly more negative values of -1.135‰ and -1.019‰ by ~8077 and ~8071 cal. years BP.

Table 1. WMC dripwater $\delta^{44/40}$Ca data. The average external 2σ over the analysis period on the standard NIST915B was 0.09‰.

Dripwater Sample	Collection Date	$\delta^{44/40}$Ca (‰ BSE)
WMC1	Mar-17	-0.29
WMC1	Jun-18	-0.42
WMC1	Feb-19	Analysis in progress
WMC1	Jun-19	Analysis in progress
WMC3	Mar-17	-0.28
WMC3	Jun-18	-0.29
WMC3	Feb-19	Analysis in progress
WMC3	Jun-19	Analysis in progress
WMC4	Feb-19	Analysis in progress
WMC4	Jun-19	Analysis in progress
WMC6	Feb-19	Analysis in progress
WMC6	Jun-19	Analysis in progress

Table 2. WMC glass plate calcite $\delta^{44/40}$Ca data. The average external 2σ over the analysis period on the standard NIST915B was 0.09‰.

Glass Plate Sample	Collection Date	$\delta^{44/40}$Ca (‰ BSE)
WMC1	Jun-18	-0.79
WMC1	Feb-19	Analysis in progress
WMC1	Jun-19	Analysis in progress
WMC2	Jun-18	-0.85
WMC3	Jun-19	Analysis in progress
WMC4	Feb-19	Analysis in progress
WMC6	Feb-19	Analysis in progress

Table 3. WMC host rock $\delta^{44/40}$Ca data. The average external 2σ over the analysis period on the standard NIST915B was 0.09‰.

Host Rock Sample	$\delta^{44/40}$Ca (‰ BSE)
WMC Mica-rich Marble	-0.59
WMC Marble with Mica Veins	-0.49
WMC Marble	-0.27

Table 4. Stalagmite WMC1 $\delta^{44/40}$Ca data. The average external 2σ over the analysis period on the standard NIST915B was 0.09‰.

Speleothem WMC1 Sample	Depth (cm)	Age (cal. years BP 1950)	$\delta^{44/40}$Ca (‰ BSE)
CD7	7.10	6852	-0.76
CD21	7.45	6897	-0.54
CD22	7.75	6936	-1.08
CD8	8.10	6983	-0.93
CD9	8.30	7009	-0.87
CD23	8.50	7035	-0.91
CD10	8.70	7061	-0.79
CD24	8.90	7088	-0.89
CD11	9.10	7114	-0.88
CD12	9.25	7134	-1.03
CD25	9.50	7166	-1.06
CD13	9.75	7199	-0.72
CD26	10.10	7245	-0.68
SC27	10.45	7290	-0.88
CD28	10.80	7337	-0.89
CD15	11.15	7382	-0.94
CD29	11.57	7435	-1.02
CD30	11.86	7472	-0.66
CD31	12.23	7521	-1.07
CD32	12.60	7571	-0.97
CD33	12.96	7622	-0.92
CD34	13.33	7678	-0.91
CD16	13.70	7737	-0.40
CD35	13.90	7769	-0.99
CD36	14.10	7800	-1.12
CD17	14.35	7839	-0.83
CD37	14.60	7875	-1.13
CD38	14.90	7916	-0.85

CD18	15.35	7968	-0.82
CD39	15.67	7998	-0.86
CD19	16.00	8023	-0.96
CD20	16.30	8041	-0.81
CD40	16.50	8052	-1.11
CD41	16.75	8062	-0.90
CD42	17.00	8071	-1.02
CD43	17.20	8077	-1.14
AC280	17.44	8082	-0.54
AC274	17.52	8084	-0.83
AC268	17.60	8086	-1.02
AC262	17.65	8087	-1.10
AC252	17.75	8089	-0.81
AC222	18.13	8097	-0.84
AC218	18.17	8098	-0.79
AC198	18.36	8103	-0.83
AC190	18.46	8105	-0.88
AC164	18.79	8116	-0.93
AC144	19.02	8126	-1.00
AC122	19.22	8137	-1.04
AC118	19.27	8140	-0.76
AC86	19.60	8162	-1.00
AC72	19.77	8175	-0.81
AC52	19.99	8193	-1.05
AC42	20.10	8203	-0.89
AC28	20.24	8214	-1.08
AC18	20.36	8226	-0.91
Cd_45	20.65	8252	-0.73
Cd_46	20.90	8276	-0.76
AC282	21.03	8284	-0.49
AC298	21.21	8304	-1.01
AC308	21.37	8318	-1.20
AC318	21.49	8329	-0.68
AC340	21.74	8351	-0.84
CD1	22.20	8390	-0.95
CD2	22.60	8422	-0.89
Cd44	23.00	8455	-1.13
CD3	23.40	8486	-1.04
CD4	23.70	8510	-1.12
CD5	24.20	8549	-1.00
CD6	24.70	8589	-1.14

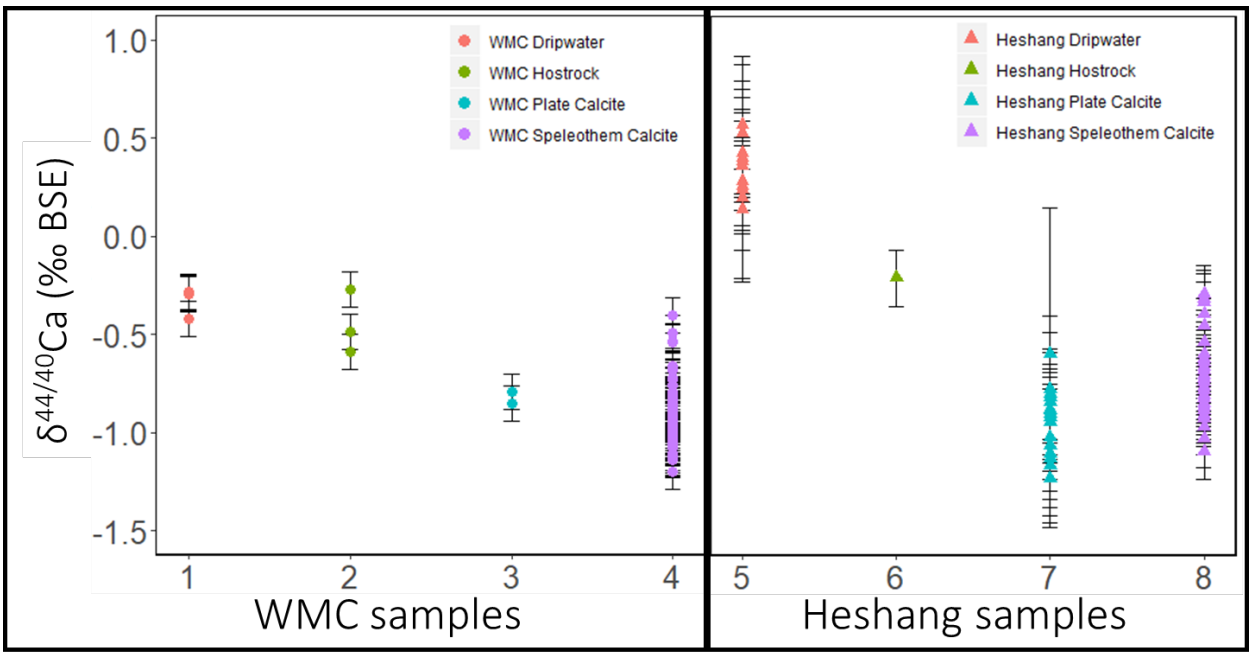

Figure 4. Distribution of $\delta^{44/40}$Ca values for WMC and Heshang Cave dripwaters, host rock, plate calcite, and speleothems. Error bars for the WMC data represent the long-term 2σ of the standard NIST915B over the analysis period of 0.9‰. Error bars for the Heshang Cave data represent the 2σ for individual samples from Owen et al. (2016). Heshang Cave data were originally reported as $\delta^{44/42}$Ca values (‰ SRM 915a). I have converted them to $\delta^{44/40}$Ca (‰ BSE).

4. DISCUSSION

4.1 Interpreting the WMC1 $\delta^{44/40}$Ca record

The WMC1 $\delta^{44/40}$Ca record is characterized by decadal to sub-decadal fluctuations throughout its entirety, with numerous rapid variations during the 8.2 kyr event as well as distributed across the record (fig. 5). In addition to changes in PCP, the observed speleothem $\delta^{44/40}$Ca variability may be partially influenced by contribution of Ca from source rocks with variable $\delta^{44/40}$Ca values or by changes to the Ca isotope fractionation factor through time (Owen et al. 2016). The range of host rock $\delta^{44/40}$Ca values at WMC means that shifts in the relative contributions of Ca from different sources cannot be completely ruled out as a potential influence on the speleothem record. The host rock samples with higher proportions of accessory mica phases tend to have more negative $\delta^{44/40}$Ca values than the sample of more pure marble (table 3). It is possible that changes in the relative dissolution of the more mica-rich marble through time could influence initial seepage water $\delta^{44/40}$Ca values and possibly explain some of the variation in the speleothem record. The marble values that we have measured vary by 0.2 to 0.3‰, which is close to the range of the 2σ variation about the mean of measured speleothem $\delta^{44/40}$Ca values (fig. 5). Some of the larger shifts in speleothem $\delta^{44/40}$Ca exceed the range of host rock variability, indicating that shifts in host rock dissolution and Ca source are not sufficient to explain the

variability in the speleothem record. Additionally, I expect that the amount of PCP can change quickly and likely in a non-unidirectional way in response to fast-paced changes in effective rainfall, whereas changes in flow path may be less responsive to these climate shifts and could be non-reversible. Nevertheless, I am currently investigating potential changes in Ca source to the speleothem through the analysis of strontium isotopes ($^{87}Sr/^{86}Sr$). Strontium ions behave similarly to Ca ions in the environment, but strontium isotopes do not fractionate during calcite precipitation and thus are not influenced by PCP (Banner et al., 1996). Comparison of these $^{87}Sr/^{86}Sr$ and $\delta^{44/40}Ca$ data should allow me to separate any effects from changing source composition in the $\delta^{44/40}Ca$ record.

The isotopic fractionation factor (α) is influenced by calcite growth rate, as controlled by saturation state (Tang et al. 2008), although the direction of this rate-dependence is still under debate (e.g. Bradbury and Turchyn 2018). This means that changes in speleothem growth rate through time could affect the speleothem $\delta^{44/40}Ca$ record. Modeled age-depth relationships show that the growth rate for stalagmite WMC1 does change over the course of the record. The growth rate increases from an average of 0.119 mm/year from 8589 to 8175 cal. years BP to an average of 0.273 mm/year from 8162 to 8041 cal. years BP and then decreases to an average of 0.076 mm/year from 8023 to 6852 cal. years BP. However, Tang et al. (2008) found that a ten-fold increase in growth rate increases $\Delta^{44/40}Ca$ by only ~0.44‰ at 25°C and Owen et al. (2016) estimate that it would take a 360-fold increase in growth rate to explain the Ca isotope excursion in the Heshang Cave record. If this sensitivity applies to WMC then I do not observe changes in growth rate over the course of the record that are sufficient to explain the magnitude of variability. For these reasons, I suggest that the observed variability in $\delta^{44/40}Ca$ over the course of the WMC1 record most likely reflects climate-driven changes to the amount of PCP through time that are being recorded by stalagmite WMC1, with less negative $\delta^{44/40}Ca$ values indicating increases in PCP and relative aridity at the time of speleothem growth.

While the WMC $\delta^{44/40}Ca$ record does display significant variability across the entirety of the record, the 8.2 kyr event appears to be unique in terms of the frequency of variations from relatively more negative to relatively less negative isotopic values. At the height of the 8.2 kyr event (~8202 to 8136 cal. years BP) speleothem $\delta^{44/40}Ca$ shows rapid oscillations, with variability between five of the six data points falling outside the uncertainty of consecutive points. Additionally, three of the most extremely negative of these data points fall below the 2σ of NIST915B from the mean of the entire dataset. Taken together, these observations point to higher variability in rainfall patterns punctuated by increases in infiltration during the height of the event. The $\delta^{44/40}Ca$ data then show a steady climb during the latter portion of the 8.2 kyr event (from ~8136 cal. years BP to ~8089) before becoming highly variable again between ~8087 and 8051 cal. years BP (fig. 5). Due to the fact that these variations are within chronological uncertainty of the extent of the 8.2 kyr event, this steady climb and subsequent return to variability may indicate either a temporary hiatus in wetness during the event or, if the high variability between ~8087 and 8051 cal. years is unrelated to the 8.2 kyr event, that the climate effects of the event at WMC were limited to the period from ~8202 to 8136 cal. years BP.

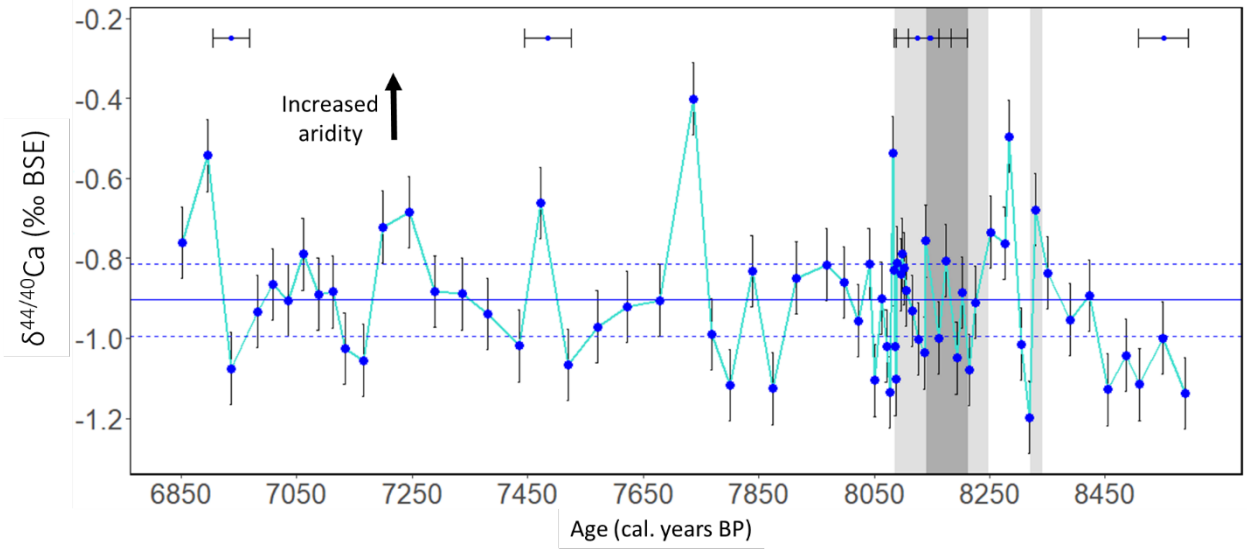

Figure 5. Timeseries of stalagmite WMC1 $\delta^{44/40}$Ca data. Error bars for $\delta^{44/40}$Ca show 2σ of the standard NIST915B over the analysis period of 0.09‰. The blue line shows the mean $\delta^{44/40}$Ca value from the record and the dashed blue lines show 2σ of NIST915B from the mean of the entire dataset. Positive excursions are interpreted as periods of increased aridity at WMC. Dark and light gray shading show the central portion and entire duration of the 8.2 kyr event as identified by Thomas et al. (2007). The earlier light gray shading shows the potential pre-cursor event proposed by Dominguez-Villar et al. (2009). Associated U-series ages and 2 sigma errors are shown at the top.

The previously published WMC1 δ^{13}C and trace element records provide an opportunity to cross-reference the possible climate signal reflected in the $\delta^{44/40}$Ca data. The WMC1 δ^{13}C record reflects changes in water supply leading to variable degassing of CO_2 and PCP in the epikarst where preferential degassing of $^{12}CO_2$ leads to higher residual $\delta^{13}C_{DIC}$ values. The WMC1 Mg/Ca record reflects changes in dissolution of Mg-rich phases in the host rock, but can also be influenced by PCP. The WMC1 P/Ca record is inversely related to the Mg/Ca and δ^{13}C data and is associated with short-lived pulses of infiltration that transport colloidal material from the soil zone above the cave to the speleothem. Together, these proxies point to intervals of increased infiltration and soil inputs to the cave and decreased host rock dissolution above the cave over the 8.2 kyr event (Oster et al., 2017). The high frequency variability and significantly negative values over the main portion of the 8.2 ky event in the WMC1 $\delta^{44/40}$Ca record support the interpretations of the WMC1 δ^{13}C and trace element records (fig. 6). If the high variability in the $\delta^{44/40}$Ca data between ~8087 and 8051 cal. years is unrelated to the 8.2 kyr event, then the duration of climate response in each proxy appears to align as well, with evidence of climate perturbation ending by ~8136 to 8120 cal. years BP in each. This indicates that climate response to the 8.2 kyr event was not as long lived at WMC as has been observed in Greenland ice cores (Thomas et al. 2007).

We may also see evidence of a short-lived precursor event to the 8.2 kyr event in the WMC1 $\delta^{44/40}$Ca record. The significant negative $\delta^{44/40}$Ca anomaly at ~8340 cal. years BP aligns with a significant negative δ^{18}O anomaly in a speleothem from Kaite Cave, Spain (fig. 7; Dominguez-Villar et al. 2009). There is also a contemporaneous negative anomaly in the WMC δ^{13}C record. Together, the negative anomalies in WMC $\delta^{44/40}$Ca and δ^{13}C indicate a short-lived period of increased wetness at ~8340 cal. years BP. The Kaite Cave speleothem δ^{18}O record is interpreted to reflect the δ^{18}O signature of the North Atlantic. The 8.2 kyr event itself is characterized by a negative δ^{18}O anomaly at Kaite Cave, and the observation of a short-lived negative anomaly that is similar in magnitude roughly 100 years prior to the onset of the 8.2 kyr event has led to the suggestion that there may have been a smaller, pre-event influx of freshwater to the North Atlantic between 8320 and 8340 cal. years BP (Dominguez-Villar 2009). It is possible that the short-lived negative anomaly that we observe is capturing climate perturbation in California related to this pre-cursor event (fig. 7).

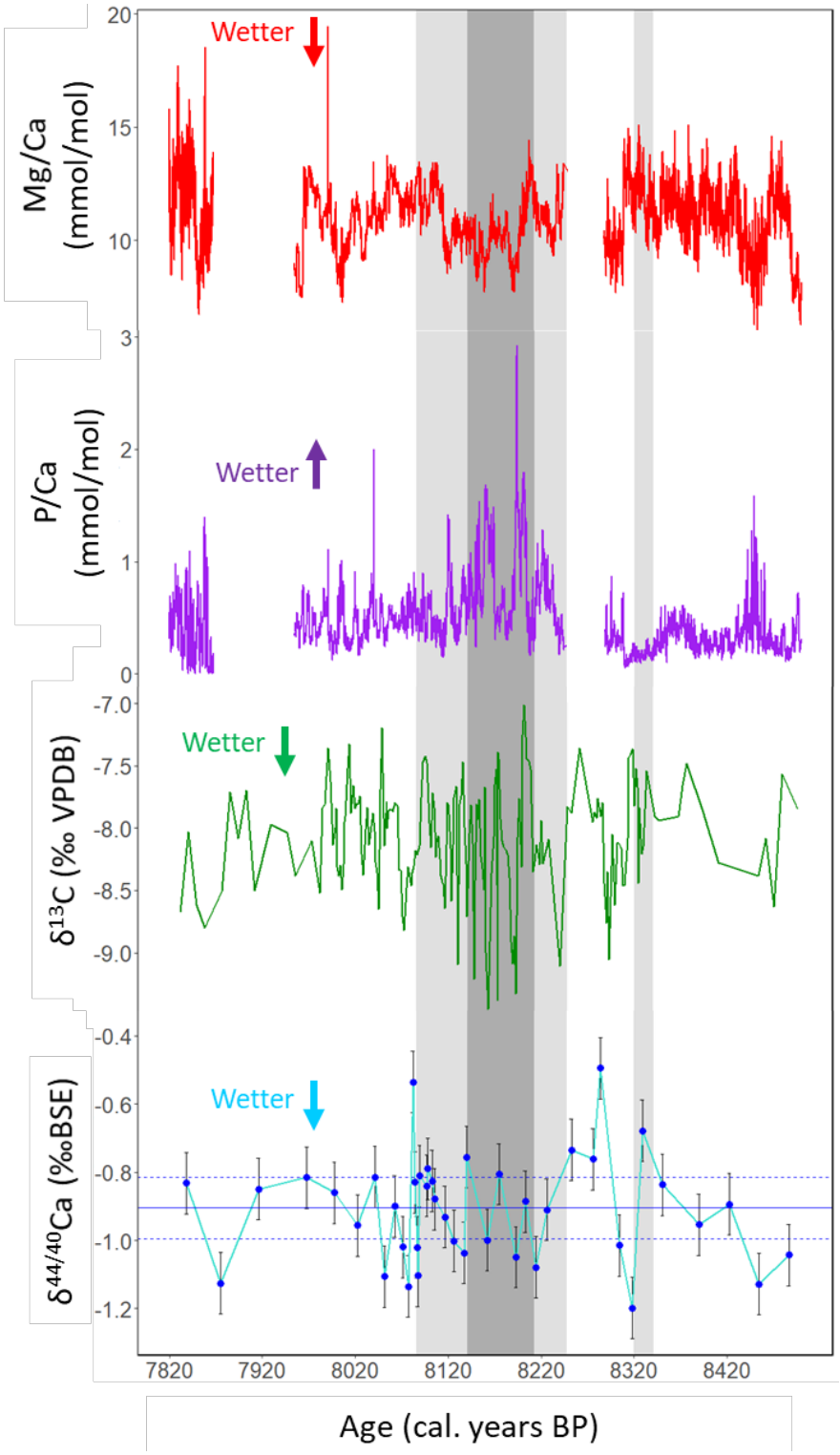

Figure 6. Timeseries of WMC1 Mg/Ca, P/Ca, $\delta^{13}C$, and $\delta^{44/40}Ca$ data over the course of the 8.2 kyr event. Dark and light gray shading show the central portion and entire duration of the 8.2 kyr event as identified by Thomas et al. (2007). The earlier light gray shading shows the potential pre-cursor event proposed by Dominguez-Villar et al. (2009).

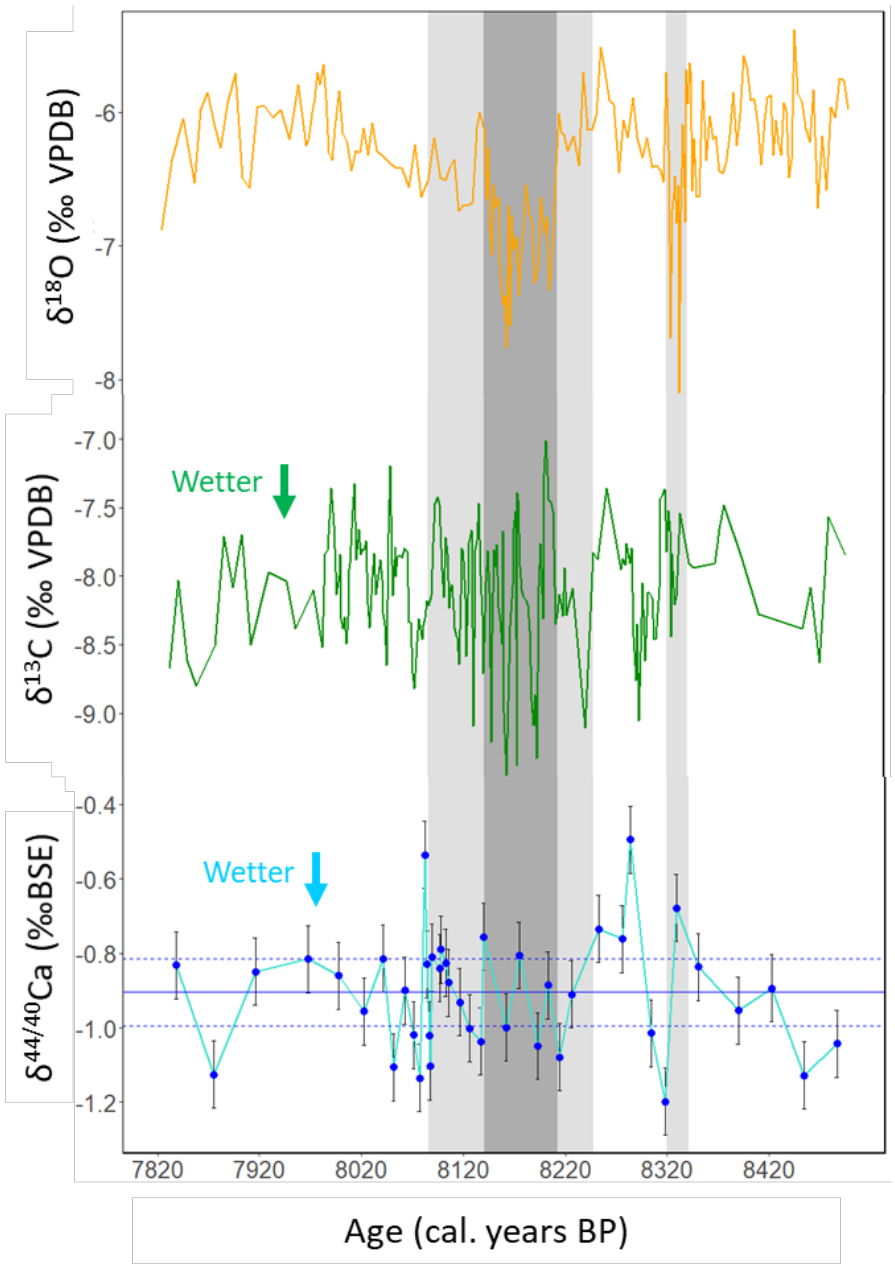

Figure 7. Timeseries of Kaite Cave $\delta^{18}O$ (Dominguez-Villar 2009) and WMC1 $\delta^{13}C$ and $\delta^{44/40}Ca$ data over the course of the 8.2 kyr event. Dark and light gray shading show the central portion and entire duration of the 8.2 kyr event as identified by Thomas et al. (2007). The earlier light gray shading shows the potential pre-cursor event proposed by Dominguez-Villar et al. (2009).

4.2 Comparisons between speleothem $\delta^{44/40}$Ca records of the 8.2 kyr event at WMC and Heshang Cave

The WMC $\delta^{44/40}$Ca records displays decadal-scale fluctuations that are of a comparable magnitude to the Heshang Cave $\delta^{44/40}$Ca record, despite the more arid climate, different bedrock geology, and potentially shorter residence time of groundwater (fig. 8). It does not show the sustained positive excursion over the course of the 8.2 kyr event displayed in the Heshang Cave record, which points to a period of prolonged aridity on the west side of the Pacific (Owen et al. 2016). Instead, the WMC $\delta^{44/40}$Ca record may show an opposite climate response – one of increase rainfall variability and over all increased wetness – in coastal California. Temporally, the WMC record shows a near-synchronous response with the Heshang Cave record, wherein $\delta^{44/40}$Ca the positive isotope excursion ends by ~8129 cal. years BP, near the middle of the later portion of the event as identified in Greenland ice cores by Thomas et al. (2007) (fig. 8).

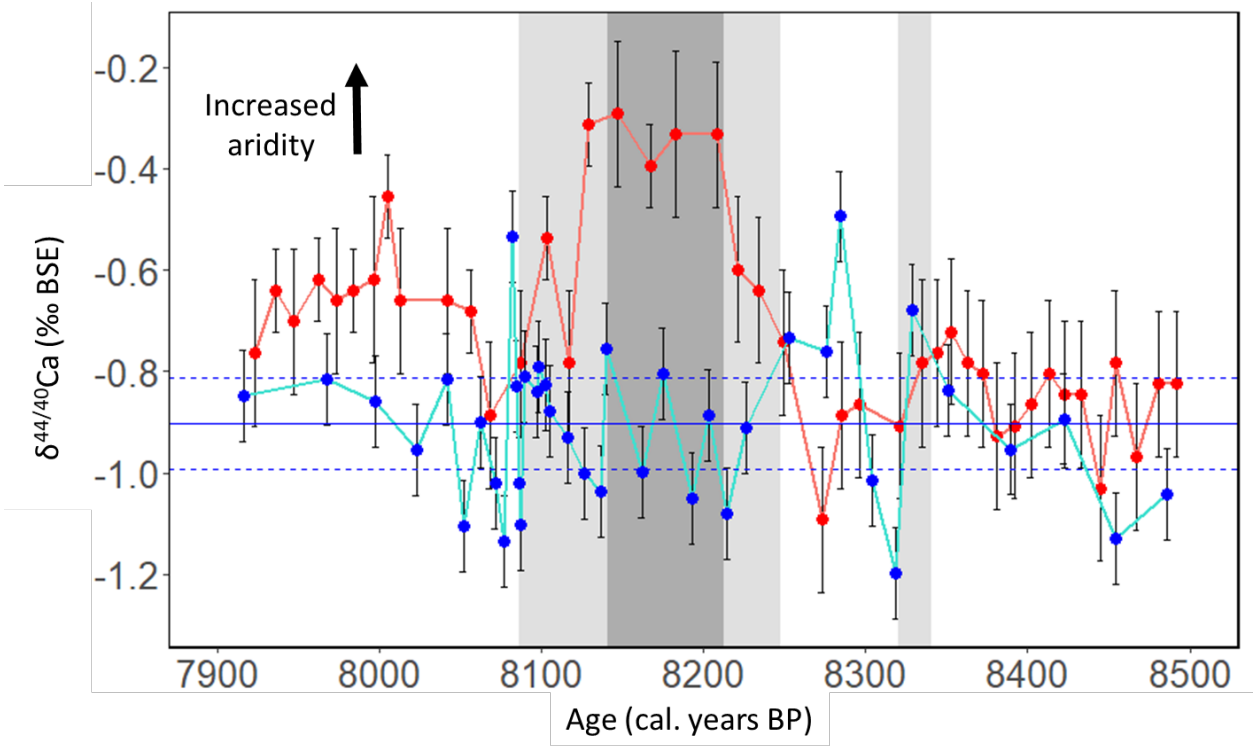

Figure 8. Timeseries of WMC1 (blue points) and Heshang Cave (red points) $\delta^{44/40}$Ca data over the 8.2 kyr event. Error bars for $\delta^{44/40}$Ca show 2σ of the standard NIST915B over the analysis period of 0.09‰. The blue line shows the mean $\delta^{44/40}$Ca value from the record and the dashed blue lines show 2σ of NIST915B from the mean of the entire dataset. Error bars for the Heshang Cave data represent the 2σ for individual samples from Owen et al. (2016). Positive excursions are interpreted as periods of increased aridity at WMC and at Heshang Cave. Dark and light gray shading show the central portion and entire duration of the 8.2 kyr event as identified by Thomas et al. (2007). The earlier light gray shading shows the potential pre-cursor event proposed by Dominguez-Villar et al. (2009).

4.3 Quantitative modeling prior calcite precipitation and rainfall amount at WMC

Speleothem $\delta^{44/40}Ca$ data can be calibrated using a simple one-box Rayleigh fractionation model of Ca cycling in the modern cave system to generate quantitative records of past rainfall (Owen et al. 2016). The model uses $\delta^{44/40}Ca$ values for groundwater in the upper epikarst following equilibration with the carbonate host rock, cave dripwater, and speleothem calcite to determine the fraction of the Ca originally dissolved in the water that remains in solution at the time when speleothem calcite is precipitated (*f*). A site-specific fractionation factor (α) that characterizes the isotopic change associated with the precipitation of calcite from an oversaturated dripwater solution can be calculated using $\delta^{44/40}Ca$ data for calcite grown in the modern environment on glass plates installed underneath drip sites (fig. 9).

Two transfer functions can be written that use measured cave system $\delta^{44/40}Ca$ data to model the evolution of dripwater and precipitate $\delta^{44/40}Ca$:

$$r_d = r_0 * f^{\alpha-1}$$

$$r_s = \alpha * r_0 * f^{\alpha-1}$$

where r_d is the Ca isotope ratio in the dripwater ($r_d = \delta_{drip}/1000+1$), r_s is the Ca isotope ratio in the precipitate from the dripwater ($r_s = \delta_{CaCO3}/1000+1$), r_0 is the initial Ca isotope ratio in the dripwater ($r_0 = \delta_{drip}{}^{f=1}/1000+1$), which is determined by the Ca isotope ratio of the host rock, α is the calculated fractionation factor for Ca between water and calcite, and *f* is the fraction of Ca remaining in solution. These equations can be rearranged to solve for *f:*

$$f = (r_d/r_0)^{1/(\alpha-1)}$$

$$f = (r_s/\alpha * r_0)^{1/(\alpha-1)}$$

for either the modern environment or for speleothem calcite using the site-specific α and inferred initial dripwater composition, r_0. This value, *f,* is interpreted as a metric for PCP (Owen et al. 2016). Once *f* is calculated, it can be used to estimate the amount of rainfall above the cave at a given time using analysis of modern drip water $\delta^{44/40}Ca$ and modern rainfall rate as a tie-point. Using this approach, rainfall is estimated to have decreased by roughly a third during the 8.2 kyr event at Heshang Cave, dropping from ~1100 mm/yr to ~700 mm/yr for ~80 years (Owen et al. 2016).

Following this approach, we calculate *f* values for each measured WMC speleothem $\delta^{44/40}Ca$ value. Given the variability in measured WMC host rock values and drip water values, I attempted several versions of the model parameterized using the different measured values for host rock and drip water in the WMC system.

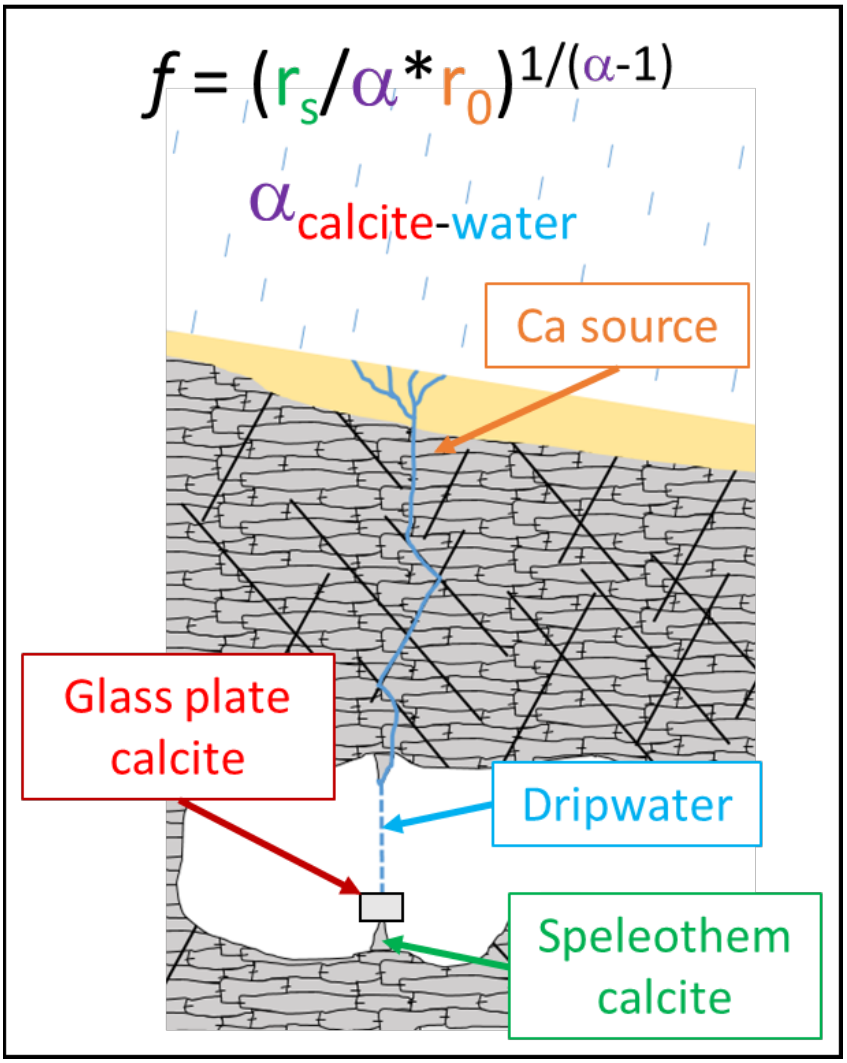

Figure 9. Schematic showing the aspects of the cave system that are inputs for the Rayleigh fractionation model and the equation for the fraction of Ca remaining in solution (*f*) based on measured speleothem $\delta^{44/40}$Ca, the $\delta^{44/40}$Ca value of the Ca source, and a site-specific fractionation factor (α).

I parameterized the model using an α value of 0.9995, calculated from drip water data collected in March 2017 and data from the glass plate that was collected in June 2018 both from drip site WMC1. I focus on this drip site, as it is the only one for which I have analyzed both drip water and glass plate calcite. I assume that the drip water data from March 2017 is characteristic of drip waters at drip site WMC1 and can be used to calculate a fractionation factor with WMC1 glass plate calcite, despite the fact that the glass plate data is an average value for the entire length of time that the plate was installed at the drip site (Feb. 2014 to June 2018). By comparison, the value for α calculated using drip water and glass plate calcite collected at drip site WMC1 in June 2018 is 0.9996. Using α = 0.9995, I calculated the fraction of Ca remaining in solution (*f*) for each measured speleothem $\delta^{44/40}$Ca value. For this, I used the minimum (-

0.586‰), maximum (-0.273‰), and mean (-0.499‰) measured host rock values as r_0. Resulting *f* values calculated using these parameterizations are shown in figure 10.

The lowest *f* values for the stalagmite are calculated using the minimum host rock value and an α value of 0.9995 and range from 0.31 to 1.23 (i.e. 31% to 123% of Ca remained in the solution at the time that that portion of the speleothem was precipitating). Using the value for α of 0.9996 calculated from June 2018 plate calcite and drip water results in higher *f* values and more speleothem measurements where *f* exceeds 1. Values for *f* that exceed 1 may indicate that Ca was not being removed from the seepage waters due to PCP. However, the results that indicate greater than 100% of the Ca dissolved from the host rock is remaining in solution at the time of speleothem precipitation suggest that further exploration into model parameterization must be done.

The complexity of the current modeled *f* values may be related to the considerable variability in WMC dripwater and host rock $\delta^{44/40}$Ca values or spatial variability in Ca isotope cycling within the epikarst. The dripwater and glass plate $\delta^{44/40}$Ca data that we have currently collected are from the upper passages of the cave, >50 feet higher than where the speleothem was collected (fig. 3A). It is possible that the length of the groundwater flow path through the epikarst plays a significant role in the amount of PCP that can occur. Thus, dripwater and glass plate $\delta^{44/40}$Ca from shallower depths may not provide an accurate calibration for speleothem $\delta^{44/40}$Ca from deeper in the cave because the flow path may be shorter in places where the epikarst is less thick. It is also possible that the Rayleigh fraction model of Owen et al. (2016) cannot be robustly applied in cave systems with less enrichment in the heavier Ca isotope in dripwaters relative to host rock during PCP, as may be the case for WMC relative to Heshang Cave (fig. 4). I expect that dripwater and glass plate data from sites WMC4 and WMC6 which are deeper within the cave and on the same level as the speleothem was collected from will serve as a better calibration for the measured speleothem $\delta^{44/40}$Ca values and will yield more realistic *f* values. Analyzing dripwater and glass plate $\delta^{44/40}$Ca from drip sites WMC4 and WMC6 will help illuminate the role that cave geometry plays in PCP and the extent to which sampling location should be considered when modeling PCP. This work represents an important next step for the development of the speleothem $\delta^{44/40}$Ca rainfall proxy and its application across diverse cave settings.

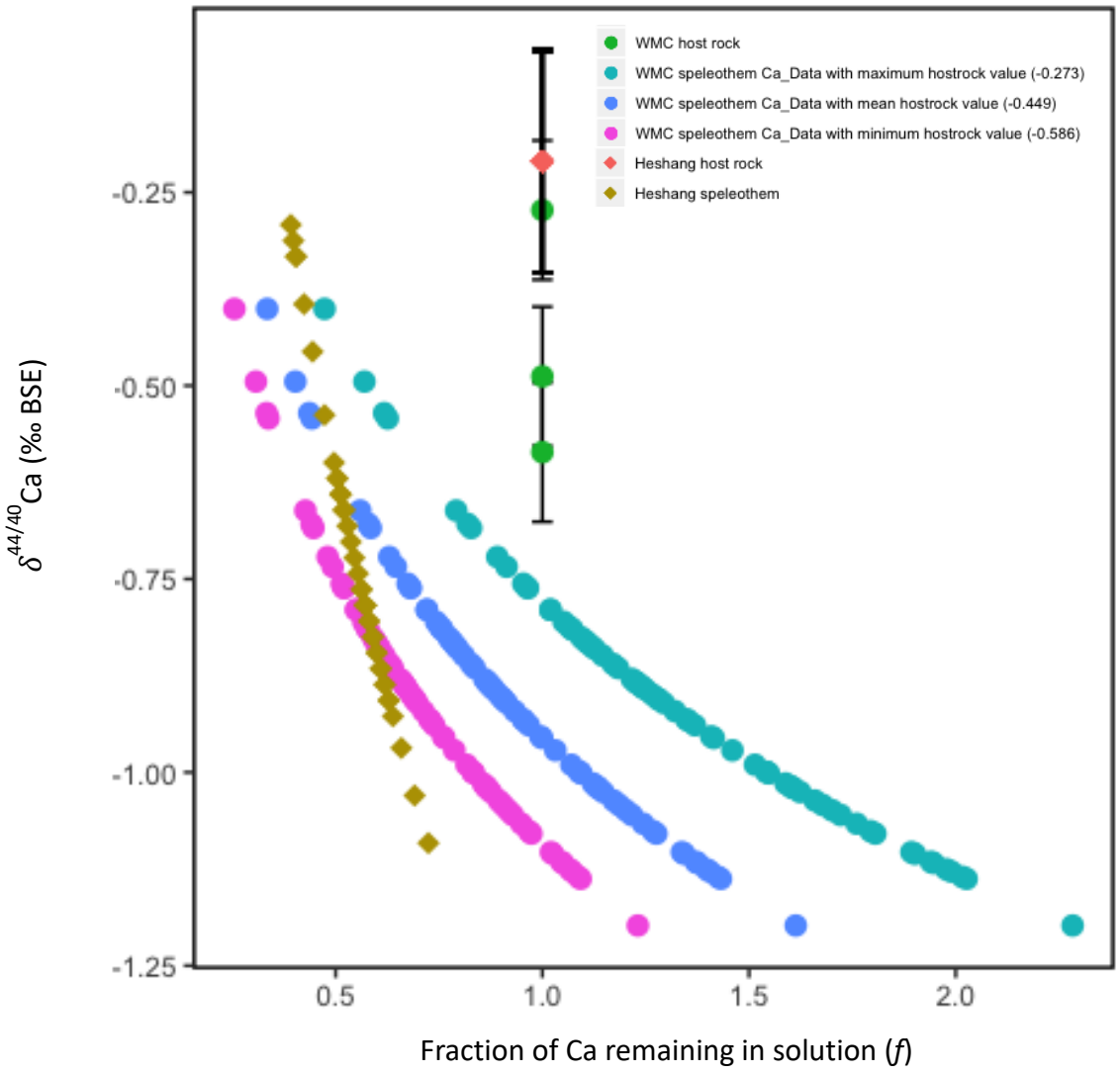

Figure 10. Modeled *f* values for measured WMC and Heshang Cave host rock and speleothem $\delta^{44/40}$Ca data. $F = 1$ represents a hypothetical solution without any Ca lost to PCP. $F = 0$ represents a solution wherein all Ca has been removed via PCP. Error bars for WMC host rock $\delta^{44/40}$Ca show 2σ of the standard NIST915B over the analysis period of 0.09‰. Error bars for the Heshang Cave host rock represent the 2σ from Owen et al. (2016).

5. CONCLUSIONS

I present the first speleothem $\delta^{44/40}Ca$ record from the western United States. The resolvable sub-decadal variations in the WMC $\delta^{44/40}Ca$ data during the 8.2 kyr event, and decadal-scale variations over the course of the entire record, suggest that this new proxy can yield useful climate information when applied in arid environments and to caves developed in fracture-dominated marble bedrock. The WMC $\delta^{44/40}Ca$ record appears to display higher frequency variability in rainfall patterns punctuated by increased in infiltration over the 8.2 kyr event relative to the rest of the record, supporting the interpretations from the WMC $\delta^{13}C$ and trace element data from Oster et al. (2017). The record does not display the sustained positive $\delta^{44/40}Ca$ excursion observable in the Heshang Cave, which suggests a weakened Asian monsoon and increased aridity in central China during the 8.2 kyr event (Owen et al. 2016). The difference between these two records may reflect a combination of difference in geology, hydrology, and mean climate that influence fluid flow through the epikarst and/or opposite climatic response to the 8.2 kyr event on either side of the Pacific Ocean.

I also apply the one-box Rayleigh fractionation model from Owen et al. (2016) to the WMC $\delta^{44/40}Ca$ record in an attempt to quantify the degree of precipitation change over the 8.2 kyr event at WMC. Using the current WMC $\delta^{44/40}Ca$ dataset we are unable to produce realistic *f* values with the Rayleigh fractionation model as many calculated *f* are greater than 1. This may be due to the considerable variability in WMC dripwater and host rock $\delta^{44/40}Ca$ values or spatial variability within the cave itself. An important next step for the development of this model will be to input dripwater and glass plate data from drip sites WMC4 and WMC6 to the model. The depths of these sites are much closer to that of the stalagmite, which may make the data from these sites more useful as model input parameters than data from drip sites that are not as deep within the cave.

The development of quantitative records of rainfall change is an important goal in paleoclimatology and the new speleothem $\delta^{44/40}Ca$ proxy and Rayleigh fractionation model show great promise in this regard. This study further develops the new speleothem $\delta^{44/40}Ca$ rainfall proxy by applying it in a novel setting and comparing it with established proxies from the same sample to assess the fidelity with which it responds to climate signals, as well as by investigating how the Rayleigh fractionation model can be best applied in new speleothem $\delta^{44/40}Ca$ studies.

REFERENCES

Arguez, A., Durre, I., Applequist, S., Squires, M., Vose, R., Yin, X., Bilotta, R., 2010, NOAA's U.S. Climate Normals (1981-2010). Santa Cruz, CA station. NOAA National Centers for Environmental Information. DOI: 10.7289/V5PN93JP. Accessed June 26, 2019.

Banner, J.L., Musgrove, M., Asmerom, Y., Edwards, R.L., and Hoff, J.A., 1996, High-resolution temporal record of Holocene ground-water chemistry: Tracing links between climate and hydrology: Geology, v. 24, p. 1049–1053, http://dx.doi.org/10.1130/0091-7613(1996)024%3C1049:HRTROH%3E2.3.CO.

Bradbury, H. and Turchyn, A., 2018, Calcium isotope fractionation in sedimentary pore fluids from ODP Leg 175: Resolving carbonate recrystallization: Geochimica et Cosmochimica Acta, v. 236, p. 121-139, doi: 10.1016/j.gca.2018.01.040

Cruz, F.W., Burns, S.J., Jercinovic, M., Karmann, I., Sharp, W.D., and Vuille, M., 2007, Evidence of rainfall variations in Southern Brazil from trace element ratios (Mg/Ca and Sr/Ca) in a Late Pleistocene stalagmite: Geochimica et Cosmochimica Acta, v. 71, p. 2250–2263, doi: 10.1016/j.gca.2007.02.005.

Dettinger, M., 2011, Climate Change, Atmospheric Rivers, and Floods in California – A Multimodel Analysis of Storm Frequency and Magnitude Changes1: JAWRA Journal of the American Water Resources Association, v. 47, p. 514–523, doi: 10.1111/j.1752-1688.2011.00546.x.

Dominguez-Villar, D., Fairchild, I.R., Baker, A., Wang, X., Edwards, L., Cheng, H. 2009, Oxygen isotope precipitation anomaly in the North Atlantic region during the 8.2 ka event: Geology, v. 37, p. 1095-1098.

Fairchild, I.J., Borsato, A., Tooth, A.F., Frisia, S., Hawkesworth, C.J., Huang, Y., McDermott, F., and Spiro, B., 2000, Controls on trace element (Sr-Mg) compositions of carbonate cave waters: Implications for speleothem climatic records: Chemical Geology, v. 166, p. 255–269, doi: 10.1016/S0009-2541(99)00216-8.

Fairchild, I.J., and Treble, P.C., 2009, Trace elements in speleothems as recorders of environmental change: Quaternary Science Reviews, v. 28, p. 449–468, doi: https://doi.org/10.1016/j.quascirev.2008.11.007.

Frisia, S., 2015, Microstratigraphic logging of calcite fabrics in speleothems as tool for palaeoclimate studies: International Journal of Speleology, v. 44, p. 1–16, doi: 10.5038/1827-806X.44.1.1.

Frisia, S., Borsato, A., Fairchild, I.J., and McDermott, F., 2000, Calcite Fabrics, Growth Mechanisms, and Environments of Formation in Speleothems from the Italian Alps and

Southwestern Ireland: Journal of Sedimentary Research, v. 70, p. 1183–1196, doi: 10.1306/022900701183.

Gussone, N., Böhm, F., Eisenhauer, A., Dietzel, M., Heuser, A., Teichert, B.M.A., Reitner, J., Wörheide, G., and Dullo, W.-C., 2005, Calcium isotope fractionation in calcite and aragonite: Geochimica et Cosmochimica Acta, v. 69, p. 4485–4494, doi: https://doi.org/10.1016/j.gca.2005.06.003.

Gussone, N., Schmitt, A.-D., Heuser, A., Wombacher, F., Dietzel, M., Tipper, E., and Schiller, M., 2016, Calcium Stable Isotope Geochemistry:, doi: 10.1007/978-3-540-68953-9.

Hu, C., Henderson, G., Huang, J., Chen, Z., Johnson, K., 2008. Report of a three year monitoring programme at Heshang Cave, Central China. International Journal of Speleology. 37, 143–151. http://dx.doi.org/10.5038/1827-806X.37.3.1.

Li, X., Cui, X., He, D., Liao, J., and Hu, C., 2018, Evaluation of the Heshang Cave stalagmite calcium isotope composition as a paleohydrologic proxy by comparison with the instrumental precipitation record: Scientific Reports, v. 8, p. 2615, doi: 10.1038/s41598-018-20776-5.

Matero, I.S.O., Gregoire, L.J., Ivanovic, R.F., Tindall, J.C., and Haywood, A.M., 2017, The 8.2 ka cooling event caused by Laurentide ice saddle collapse: Earth and Planetary Science Letters, v. 473, p. 205–214, doi: 10.1016/j.epsl.2017.06.011.

Morrill, C., Anderson, D.M., Bauer, B.A., Buckner, R., Gille, E.P., Gross, W.S., Hartman, M., and Shah, A., 2013, Proxy benchmarks for intercomparison of 8.2 ka simulations: Climate of the Past, v. 9, p. 423–432, doi: 10.5194/cp-9-423-2013.

Morrill, C., Legrande, A.N., Renssen, H., Bakker, P., and Otto-Bliesner, B.L., 2013, Model sensitivity to North Atlantic freshwater forcing at 8.2 ka: Climate of the Past, v. 9, p. 955–968, doi: 10.5194/cp-9-955-2013.

Oster, J.L., Sharp, W.D., Covey, A.K., Gibson, J., Rogers, B., and Mix, H., 2017, Climate response to the 8.2 ka event in coastal California: Scientific Reports, v. 7, p. 3886, doi: 10.1038/s41598-017-04215-5.

PRISM Climate Group, Oregon State University, http://prism.oregonstate.edu.

Reynard, L.M., Day, C.C., and Henderson, G.M., 2011, Large fractionation of calcium isotopes during cave-analogue calcium carbonate growth: Geochimica et Cosmochimica Acta, v. 75, p. 3726–3740, doi: 10.1016/j.gca.2011.04.010.

Scholz, D., and Hoffmann, D.L., 2011, StalAge – An algorithm designed for construction of speleothem age models: Quaternary Geochronology, v. 6, p. 369–382, doi: https://doi.org/10.1016/j.quageo.2011.02.002.

Tang, J.W., Dietzel, M., Bohm, F., Kohler, S.J., and Eisenhauer, A., 2008, Sr2+/Ca2+ and Ca-44/Ca-40 fractionation during inorganic calcite formation: II. Ca isotopes: Geochimica et Cosmochimica Acta, v. 72, p. 3733–3745, doi: 10.1016/j.gca.2008.05.033.

Tooth, Anna F.; Fairchild, Ian, J., 2003, Soil and karst aquifer hydrological controls on the geochemical evolution of speleothem-forming drip waters, Crag Cave, southwest Ireland: Journal of Hydrology, v. 273, p. 51–68, doi: 10.1016/S0022-1694(02)00349-9.

Tremaine, D.M., and Froelich, P.N., 2013, Speleothem trace element signatures: A hydrologic geochemical study of modern cave dripwaters and farmed calcite: Geochimica et Cosmochimica Acta, v. 121, p. 522–545, doi: 10.1016/j.gca.2013.07.026.

Thomas, E.R., Wolff, E.W., Mulvaney, R., Steffensen, J.P., Johnsen, S.J., Arrowsmith, C., White, J.W.C., Vaughn, B., Popp, T., 2007, The 8.2ka event from Greenlnd ice cores: Quarternary Science Reviews, v. 26, p. 70-81.

Warken, S.F., Fohlmeister, J., Schröder-Ritzrau, A., Constantin, S., Spötl, C., Gerdes, A., Esper, J., Frank, N., Arps, J., Terente, M., Riechelmann, D.F.C., Mangini, A., and Scholz, D., 2018, Reconstruction of late Holocene autumn/winter precipitation variability in SW Romania from a high-resolution speleothem trace element record: Earth and Planetary Science Letters, v. 499, p. 122–133, doi: 10.1016/j.epsl.2018.07.027.

Wiersma, A.P., and Renssen, H., 2006, Model–data comparison for the 8.2kaBP event: confirmation of a forcing mechanism by catastrophic drainage of Laurentide Lakes: Quaternary Science Reviews, v. 25, p. 63–88, doi: https://doi.org/10.1016/j.quascirev.2005.07.009.

Wong, C.I., and Breecker, D.O., 2015, Advancements in the use of speleothems as climate archives: Quaternary Science Reviews, v. 127, p. 1–18, doi: 10.1016/j.quascirev.2015.07.019.